Supporting Information for "Variability in Biomass Burning Emissions Weakens Aerosol Forcing"

Kyle B. Heyblom[1], Hansi A. Singh[1], Philip J. Rasch[2], Haruki Hirasawa[1]

[1]School of Earth and Ocean Sciences, University of Victoria, Victoria, BC, Canada

[2]Department of Atmospheric Science, University of Washington, Seattle, WA, USA

Contents of this file

Introduction

Text S1. CESM2 Large Ensemble. The Community Earth System Model version 2 Large Ensemble (CESM2-LE) is a project which contains data from 100 total ensemble members using CESM2 with historical forcing from 1850 to 2014 and future SSP3-7.0 (a medium-to-high emissions scenario) forcing from 2015 to 2100 (Rodgers et al., 2021; O'Neill et al., 2016). 50 ensemble members (of the total 100) were forced with the biomass burning (BB) emissions prescribed for CMIP6 historical and SSP3-7.0 scenario simulations. The other 50 ensemble members were forced with temporally smoothed BB emissions during the late historical and early future projection periods, achieved with an 11-year running mean filter from 1990 to 2020. This smoothing reduces temporal variability in this ensemble set, but nearly preserves total emissions compared to the ensemble

January 5, 2023, 1:17am

set containing the higher BB emissions variability (Rodgers et al., 2021). Each of the 100 ensemble members were simulated using a fully coupled configuration of CESM2 which is comprised of the Community Atmosphere Model version 6 (CAM6; Danabasoglu et al., 2020), Parallel Ocean Program version 2 (POP2; Smith et al., 2010), Los Alamos Sea Ice Model version 5.1.2 (CICE5; Hunke et al., 2015), and Community Land Model version 5 (CLM5; Lawrence et al., 2019). Aerosols were simulated using the four-mode version of the Modal Aerosol Module (MAM4; Liu et al., 2016). Each component was configured at a nominal 1° spatial resolution (Rodgers et al., 2021). Each individual ensemble member was initialized using a combination of micro perturbations to the temperature field and macro perturbations based on different phases of the Atlantic Meridional Overturning Circulation strength (Rodgers et al., 2021). We evaluate the impact of BB emissions variability (Figures 1 and 4) as the difference between the ensemble mean of the high BB emissions variability members and of the low BB emissions variability members, unless otherwise specified.

Text S2. Forcing Calculation. We approximate the effective radiative forcing (ERF) by running simulations in CESM2 with fixed sea surface temperatures (SSTs). By holding SSTs constant, we remove most climate feedbacks by preventing the surface temperature from changing (Hansen et al., 2005; Forster et al., 2021). The land surface, however, is still active in our simulations, and thus able to change temperature in the presence of a forcing. We adjust our ERF approximation for changes in land temperature by approximating the Planck feedback due to this land temperature change using a radiative kernel, as recommended by Forster et al. (2021). We use the land radiative kernel provided

by Pendergrass, Conley, and Vitt (n.d.). We thus use the following to calculate the ERF:

$$ERF = \Delta F_{fSST} - k\Delta T_{land} \tag{1}$$

Where ΔF_{fSST} is the change in net radiation flux at the top of atmosphere, k is the land radiation kernel, and ΔT_{land} is the change in land surface temperature. Differences are taken as the difference between high BB emissions variability scenarios (i.e., Real-Var and Pulse-Var) and the zero interannual variability baseline (Zero-Var).

Text S3. Aquaplanet Simulations. To evaluate if the observed response in clouds to changes in BB emissions variability is the result of land surface feedbacks, we simulate the Real-Var and Zero-Var scenarios using an aquaplanet configuration with CESM2. The aquaplanet simulations have no topography, land, or sea ice (i.e., are entirely covered by oceans), but otherwise use the same boundary conditions as our idealized fixed-SST simulations (see Section 2). Additionally, SSTs are prescribed to vary only with latitude and the orbital parameters are set to perpetual equinox conditions (Neale & Hoskins, 2000).

Text S4. Idealized Aerosol-CRE Response. Figure 5 shows how the nonlinearity in the aerosol-CRE relationship results in a weakening of the magnitude (less negative) of CRE when there is greater aerosol emissions variability. Panel (a) in Figure 5 shows probability density functions (PDF) of aerosol concentrations that are representative of the Zero-Var (black) and Real-Var (green). The idealized aerosol PDFs are determined by fitting normal and log-normal distributions to the June–September (JJAS) mean aerosol concentrations averaged from Zero-Var and Real-Var simulations, respectively, averaged over 50–70°N. Panel (b) shows idealized CRE responses to aerosol concentration. The

solid purple line shows a realistic nonlinear aerosol-CRE response, determined by fitting a logarithmic curve to the JJAS 50–70°N mean CRE responses to aerosol concentrations from all experiments used in this study (and shown in Figure 4, except the CESM2-LE). The nonlinear aerosol-CRE response is represented by the following equation (where a, b, c are fit constants):

$$CRE = a \cdot \ln\left(Aer + b\right) + c \tag{2}$$

The dashed purple lines shows a theoretical linear aerosol-CRE response, representative of an assumption that emissions variability has no effect on the time-averaged CRE response. The linear aerosol-CRE response is determined by fitting a linear curve to the JJAS 50–70°N mean CRE responses to aerosol concentrations from the Real-Var. The nonlinear aerosol-CRE response is represented by the following equation (where d, e are fit constants):

$$CRE = d \cdot Aer + e \tag{3}$$

Panel (c) shows the resulting CRE PDFs from the normal and log-normal aerosol concentration PDFs. Solid (dashed) CRE PDFs show the transformation due to the nonlinear (linear) aerosol-CRE responses. Nonlinear CRE PDF transformations were performed by:

$$PDF_{CRE} = |\frac{Aer + b}{a}| \cdot PDF_{Aer} \tag{4}$$

Linear CRE PDF transformations were performed by:

$$PDF_{CRE} = |\frac{1}{a}| \cdot PDF_{Aer} \tag{5}$$

Panel (d) shows a time series of aerosol concentrations comprised of 100 randomly selected years from the normal and log-normal aerosol concentration PDFs (black and green lines,

respectively). Panel (e) shows the corresponding CRE responses to the aerosol concentrations in panel (d). Solid (dashed) lines in panel (e) represent the response due to the nonlinear (linear) aerosol-CRE curves shown in panel (b).

Text S5. CMIP6-AMIP Data. We use Coupled Model Intercomparison Project Phase 6 (CMIP6) Atmospheric Model Intercomparison Project (AMIP) historical simulations to evaluate whether characteristic aerosol-cloud interaction nonlinearities can be found in other Earth System Models (ESMs; Figure S7). We use all data available at the time of writing to compute the cloud radiative effect. The models (number of ensemble members) used are as follows: ACCESS-ESM1-5 (1), BCC-CSM2-MR (1), BCC-ESM1 (1), CAMS-CSM1-0 (3), CanESM5 (7), CESM2 (2), CESM2-FV2 (1), CESM2-WACCM (3), CESM2-WACCM-FV2 (1), CNRM-CM6-1 (1), CNRM-CM6-1-HR (1), CNRM-ESM2-1 (1), E3SM-1-0 (2), EC-Earth3-Veg (1), FGOALS-f3-L (3), GFDL-AM4 (1), GFDL-CM4 (1), GISS-E2-1-G (15), GISS-E2-2-G (1), HadGEM3-GC31-LL (5), HadGEM3-GC31-MM (2), INM-CM4-8 (1), INM-CM5-0 (1), IPSL-CM6A-LR (11), KACE-1-0-G (1), MIROC6 (10), MPI-ESM1-2-HR (1), MRI-ESM2-0 (3), NESM3 (5), NorCPM1 (1), NorESM2-LM (1), SAM0-UNICON (1), UKESM1-0-LL (2). Results are evaluated by pooling all ensemble members together. Cloud radiative effects simulated by each CMIP6-AMIP model are evaluated against the the CMIP6 prescribed BB emissions(van Marle et al., 2017).

Text S6. Evaluating Statistically-Robust Evidence of Emissions-CRE Nonlinearity. We categorize the response of cloud radiative effect (CRE) to biomass burning (BB) emissions to have statistically-robust evidence of the expected nonlinear response

(based on CESM2 results; see Figure 4b; and past observational evidence (Twomey, 1977; Rissman et al., 2004; Reutter et al., 2009; Bougiatioti et al., 2016; Kacarab et al., 2020)) if the following criteria are met: (1) if the P-value of both (low and high BB emissions value) regression slopes are less than 0.1; (2) if the P-value of the difference in slopes is less than 0.1; (3) if both slopes values are negative; (4) if the slope of the regression over low BB emissions values is more negative than the slope of the regression over high BB emissions values.

Text S7. Evaluating Spatial Statistical Significance. We use a Welch's t-test to assess the the statistical significance of differences at spatial scales (i.e., grid point; shown in figures as stippling). We additionally limit significance determinations for false discoveries (Wilks, 2016). We use an α_{FDR} of 0.20 to approximate a global significance level of 0.1.

References

Bougiatioti, A., Bezantakos, S., Stavroulas, I., Kalivitis, N., Kokkalis, P., Biskos, G., . . . Nenes, A. (2016). Biomass-burning impact on CCN number, hygroscopicity and cloud formation during summertime in the eastern Mediterranean. *Atmospheric Chemistry and Physics*, *16*(11), 7389–7409. doi: 10.5194/acp-16-7389-2016

Danabasoglu, G., Lamarque, J.-F., Bacmeister, J., Bailey, D. A., DuVivier, A. K., Edwards, J., . . . Strand, W. G. (2020). The Community Earth System Model Version 2 (CESM2). *Journal of Advances in Modeling Earth Systems*, *12*(2), e2019MS001916. doi: 10.1029/2019MS001916

Forster, P., Storelvmo, T., Armour, K., Collins, W., Dufresne, J.-L., Frame, D., . . .

Zhang, H. (2021). The Earth's Energy Budget, Climate Feedbacks, and Climate Sensitivity. In V. Masson-Delmotte et al. (Eds.), *Climate Change 2021: The Physical Science Basis. Contribution of Working Group I to the Sixth Assessment Report of the Intergovernmental Panel on Climate Change* (pp. 923–1054). Cambridge, United Kingdom and New York, NY, USA: Cambridge University Press. doi: 10.1017/9781009157896.009

Hansen, J., Sato, M., Ruedy, R., Nazarenko, L., Lacis, A., Schmidt, G. A., . . . Zhang, S. (2005). Efficacy of climate forcings. *Journal of Geophysical Research: Atmospheres*, *110*(D18). doi: 10.1029/2005JD005776

Hunke, E. C., Lipscomb, W. H., Turner, A. K., Jeffery, N., & Elliot, S. (2015). *CICE: The los alamos sea ice model documentation and software user's manual version 5.1* (Tech. Rep. No. LA-CC-06-012). Los Alamos National Laboratory.

Kacarab, M., Thornhill, K. L., Dobracki, A., Howell, S. G., O'Brien, J. R., Freitag, S., . . . Nenes, A. (2020). Biomass burning aerosol as a modulator of the droplet number in the southeast Atlantic region. *Atmospheric Chemistry and Physics*, *20*(5), 3029–3040. doi: 10.5194/acp-20-3029-2020

Lawrence, D. M., Fisher, R. A., Koven, C. D., Oleson, K. W., Swenson, S. C., Bonan, G., . . . Zeng, X. (2019). The community land model version 5: Description of new features, benchmarking, and impact of forcing uncertainty. *Journal of Advances in Modeling Earth Systems*, *11*(12), 4245–4287. doi: 10.1029/2018MS001583

Liu, X., Ma, P. L., Wang, H., Tilmes, S., Singh, B., Easter, R. C., . . . Rasch, P. J. (2016). Description and evaluation of a new four-mode version of the Modal Aerosol Module (MAM4) within version 5.3 of the Community Atmosphere Model. *Geoscientific*

Model Development, *9*(2), 505–522. doi: 10.5194/gmd-9-505-2016

Neale, R. B., & Hoskins, B. J. (2000). A standard test for AGCMs including their physical parametrizations: I: The proposal. *Atmospheric Science Letters*, *1*(2), 101–107. doi: 10.1006/asle.2000.0022

O'Neill, B. C., Tebaldi, C., van Vuuren, D. P., Eyring, V., Friedlingstein, P., Hurtt, G., ... Sanderson, B. M. (2016). The Scenario Model Intercomparison Project (ScenarioMIP) for CMIP6. *Geoscientific Model Development*, *9*(9), 3461–3482. doi: 10.5194/gmd-9-3461-2016

Pendergrass, A. G., Conley, A., & Vitt, F. M. (n.d.). Surface and top-of-atmosphere radiative feedback kernels for CESM-CAM5. *m K*, 8.

Reutter, P., Su, H., Trentmann, J., Simmel, M., Rose, D., Gunthe, S. S., ... Poschl, U. (2009). Aerosol- and updraft-limited regimes of cloud droplet formation: Influence of particle number, size and hygroscopicity on the activation of cloud condensation nuclei (CCN). *Atmos. Chem. Phys.*, 14.

Rissman, T. A., Nenes, A., & Seinfeld, J. H. (2004). Chemical Amplification (or Dampening) of the Twomey Effect: Conditions Derived from Droplet Activation Theory. *Journal of the Atmospheric Sciences*, *61*(8), 919–930. doi: 10.1175/ 1520-0469(2004)061⟨0919:CAODOT⟩2.0.CO;2

Rodgers, K. B., Lee, S.-S., Rosenbloom, N., Timmermann, A., Danabasoglu, G., Deser, C., ... Yeager, S. G. (2021). Ubiquity of human-induced changes in climate variability. *Earth System Dynamics*, *12*(4), 1393–1411. doi: 10.5194/esd-12-1393-2021

Smith, R., Jones, P., Briegleb, B., Bryan, F., Danabasoglu, G., Dennis, J., ... Yeager, S. (2010). The Parallel Ocean Program (POP) reference, manual ocean component

of the Community Climate System Model (CCSM) and Community Earth System Model (CESM). *LANL Tech. Report*.

Twomey, S. (1977). The Influence of Pollution on the Shortwave Albedo of Clouds. *Journal of Atmospheric Sciences*, *34*(7), 1149–1152. doi: 10.1175/1520-0469(1977) 034⟨1149:TIOPOT⟩2.0.CO;2

van Marle, M. J. E., Kloster, S., Magi, B. I., Marlon, J. R., Daniau, A.-L., Field, R. D., . . . van der Werf, G. R. (2017). Historic global biomass burning emissions for CMIP6 (BB4CMIP) based on merging satellite observations with proxies and fire models (1750–2015). *Geoscientific Model Development*, *10*(9), 3329–3357. doi: 10.5194/gmd-10-3329-2017

Wilks, D. S. (2016). "The Stippling Shows Statistically Significant Grid Points": How Research Results are Routinely Overstated and Overinterpreted, and What to Do about It. *Bulletin of the American Meteorological Society*, *97*(12), 2263–2273. doi: 10.1175/BAMS-D-15-00267.1

a) **Real-Var:** *Annual*
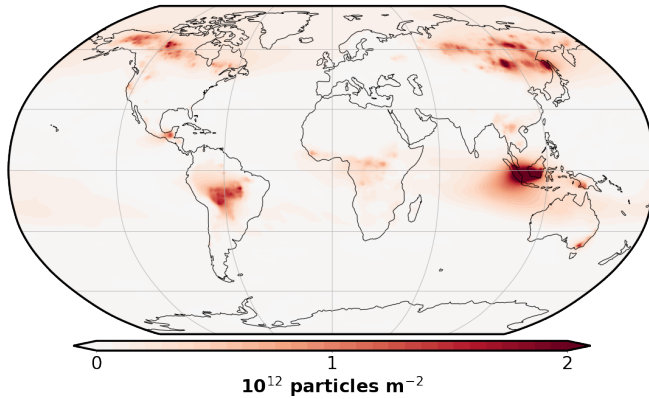
b) **Real-Var:** *JJAS*
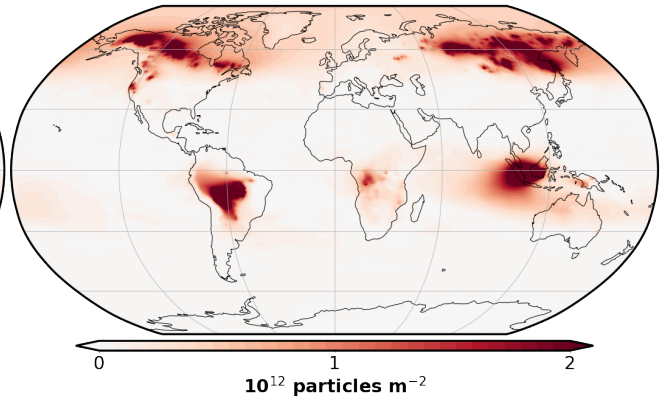
c) **Pulse-Var:** *Annual*
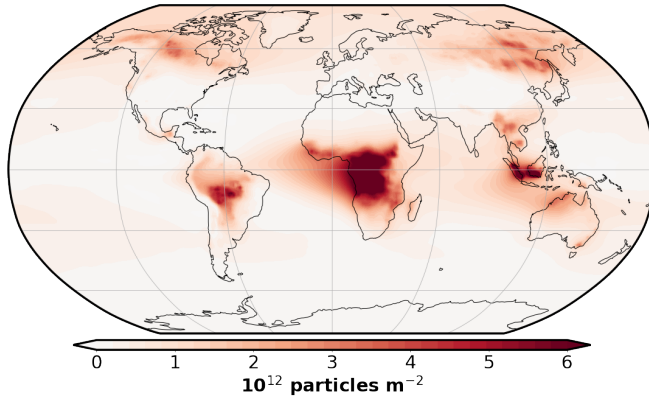
d) **Pulse-Var:** *JJAS*
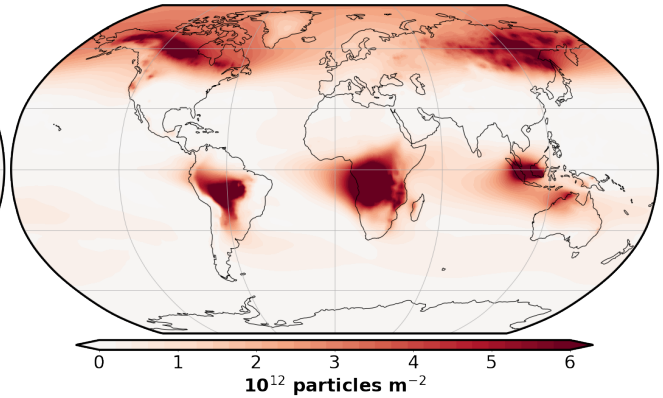
Figure S1. **Variability of biomass burning (BB) emissions prescribed in each idealized experiment.** Shown is the standard deviation of BB emissions (in 10^{12} particles m^{-2}) in the Real-Var (a and b) and Pulse-Var (c and d) experiments for annual (a and c) and June–September (JJAS; b and d) means.
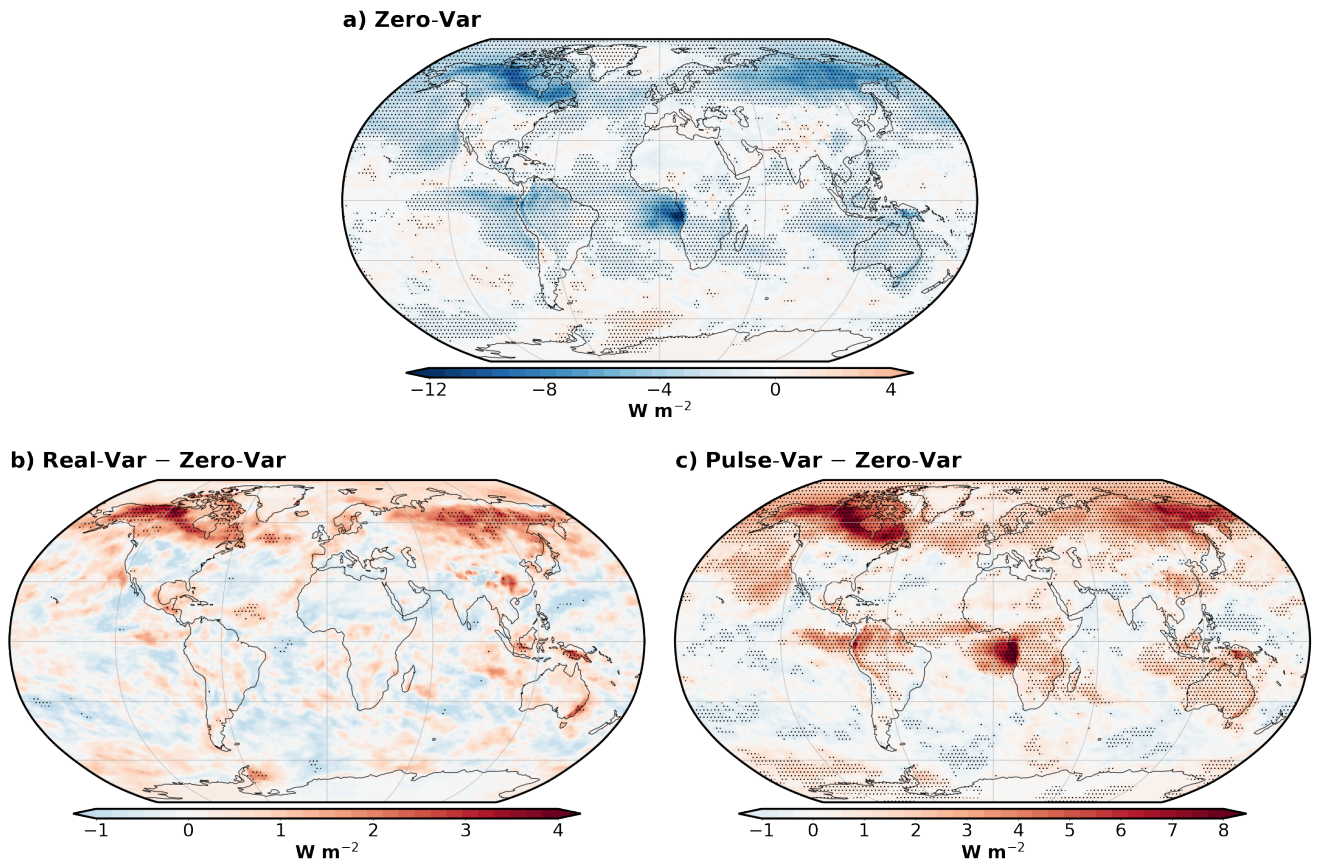
Figure S2. **Change in annual effective radiative forcing due to biomass burning emissions variability ($\Delta\mathrm{ERF}_{\mathrm{BBVar}}$).** Panel (a) shows the absolute ERF due to BB emissions in the Zero-Var experiment (relative to no BB emissions). $\Delta\mathrm{ERF}_{\mathrm{BBVar}}$ is shown for the Real-Var (Panel (b)) and Pulse-Var (Panel (c)) experiments. $\Delta\mathrm{ERF}_{\mathrm{BBVar}}$ is defined as the variability experiments minus the Zero-Var experiment. The left (right) column shows the annual (June–September; JJAS) mean change. Stippling signifies 90% confidence (see Text S7).
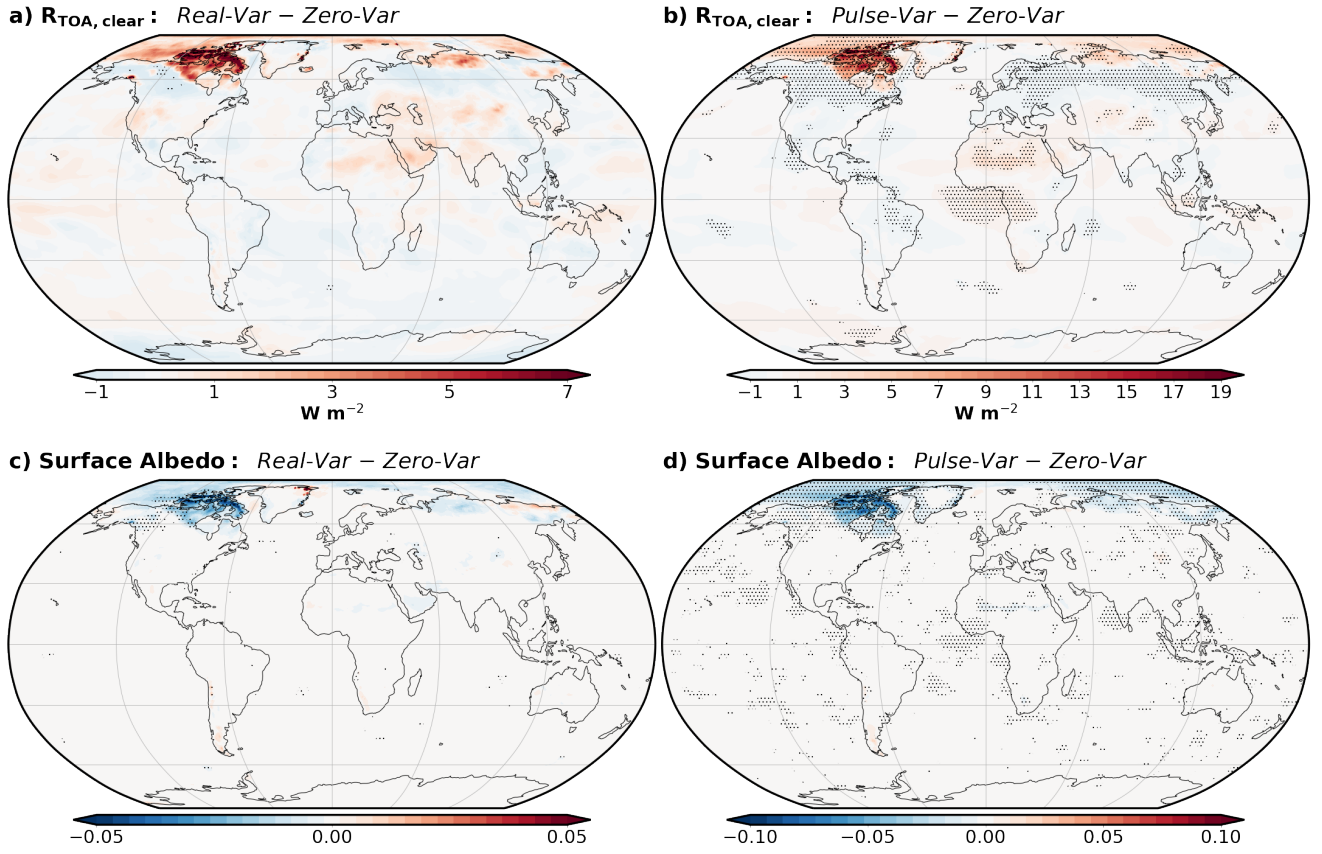
a) CDNC : *Real-Var − Zero-Var*
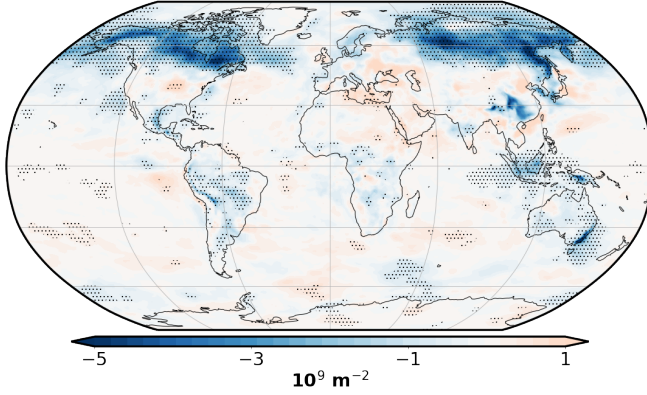
b) CDNC : *Pulse-Var − Zero-Var*
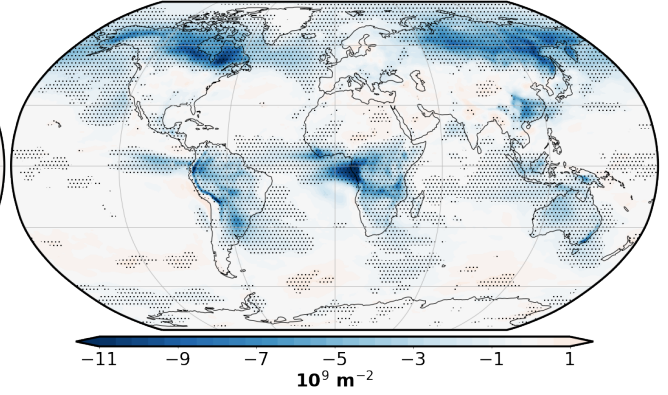
c) CRE : *Real-Var − Zero-Var*
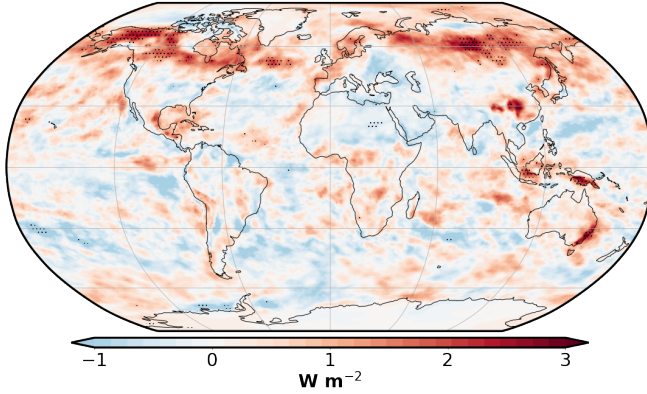
d) CRE : *Pulse-Var − Zero-Var*
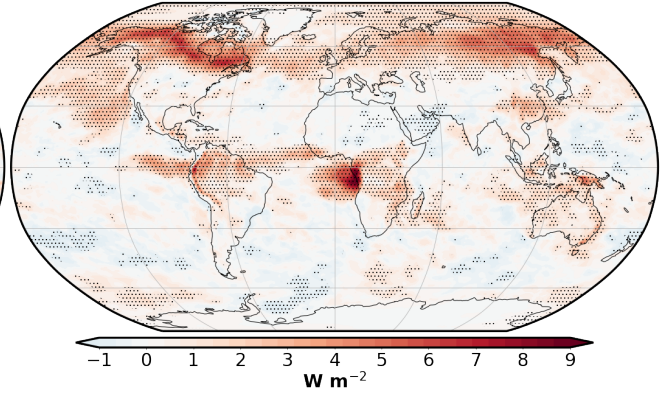
Figure S3.   Annual mean change in cloud properties due to biomass burning (BB) emissions variability. Annual mean change in cloud droplet number concentration (CDNC; in 10^9 m^{-2}; (a) and (b)) and cloud radiative effect (CRE; in W m^{-2}; (c) and (d)) due to BB emissions variability in the Real-Var (left column) and Pulse-Var (right column) experiments. Changes due to BB emissions variability are defined as the variability experiments minus the Zero-Var experiment. Stippling signifies 90% confidence (see Text S7).
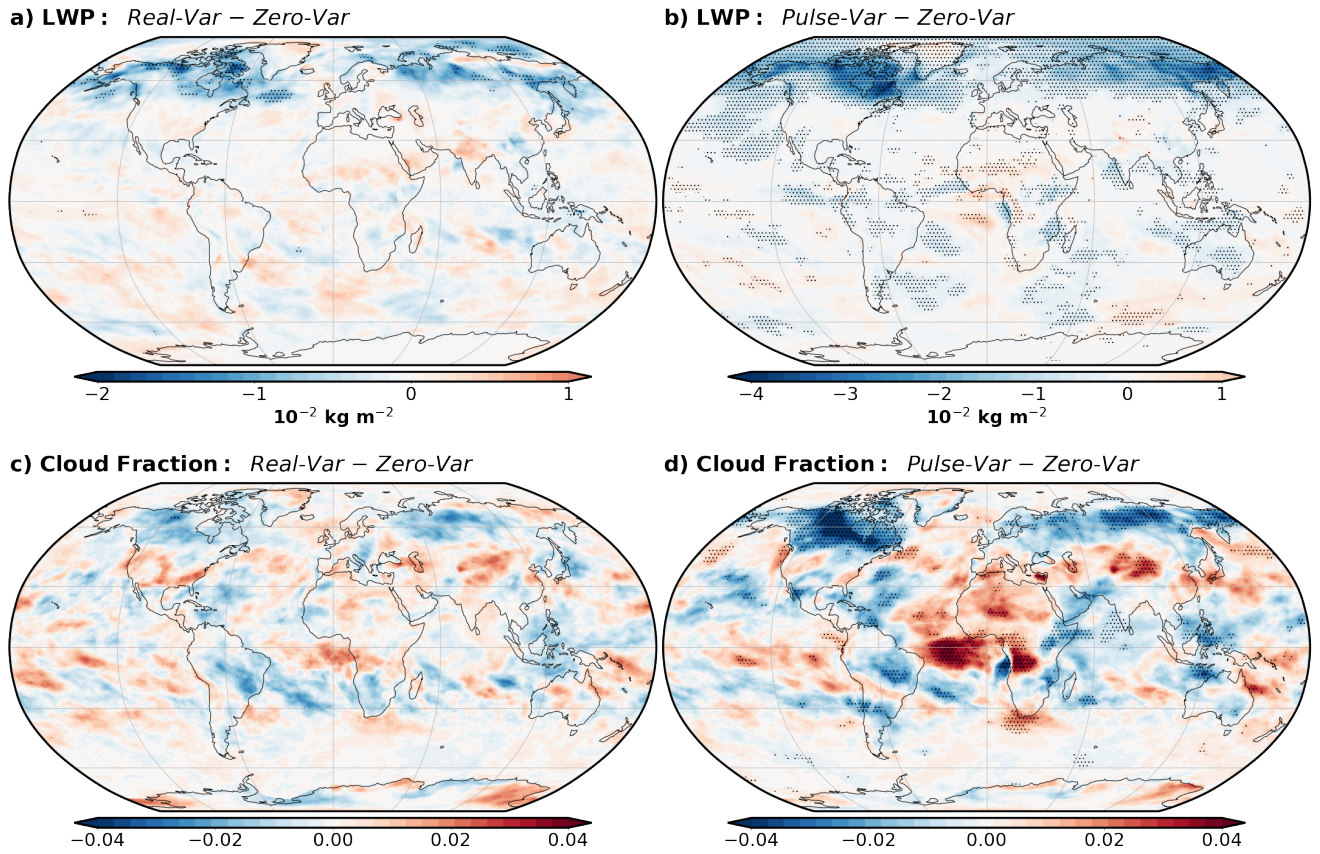
Figure S4. **Change in cloud amount due to biomass burning (BB) emissions variability.** June–September (JJAS) mean change in liquid water path (LWP; in 10^{-2} kg m^{-2}; (a) and (b)) and fraction ((c) and (d)) due to BB emissions variability in the Real-Var (a) and Pulse-Var (b) experiments. Changes due to BB emissions variability are defined as the variability experiments minus the Zero-Var experiment. Stippling signifies 90% confidence (see Text S7).

a) R$_{\text{TOA, clear}}$: *Real-Var − Zero-Var*

b) R$_{\text{TOA, clear}}$: *Pulse-Var − Zero-Var*

W m^{-2}

W m^{-2}

c) Surface Albedo : *Real-Var − Zero-Var*

d) Surface Albedo : *Pulse-Var − Zero-Var*

Figure S5. **Change in clear-sky top of atmosphere net radiative flux ($R_{TOA,clear}$) and surface albedo due to biomass burning (BB) emissions variability.** As in Figure S4 but for $R_{TOA,clear}$ (in W m^{-2}; (a) and (b)) and surface albedo ((c) and (d)).

a) CDNC : *Real-Var − Zero-Var*

b) CRE : *Real-Var − Zero-Var*
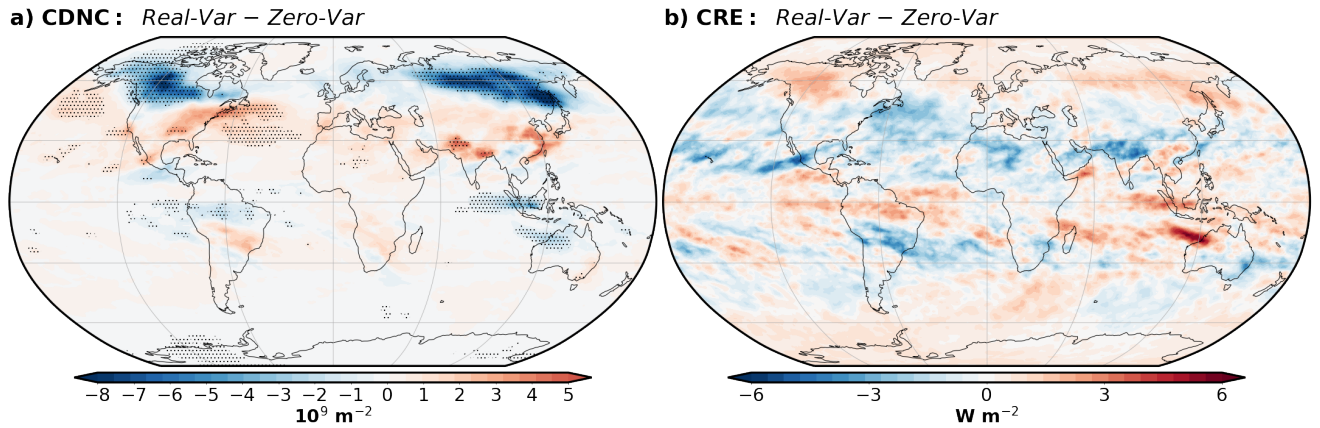
Figure S6. **Change in cloud properties due to biomass burning (BB) emissions variability in aquaplanet simulations.** June–September (JJAS) mean change in cloud droplet number concentration (CDNC; in 10^9 m^{-2}; (a)) radiative effect (CRE; in W m^{-2}; (c)) due to BB emissions variability in the Real-Var experiment in an aquaplanet simulation. Changes due to BB emissions variability are defined as the variability experiments minus the Zero-Var experiment. Stippling signifies 90% confidence (see Text S7).
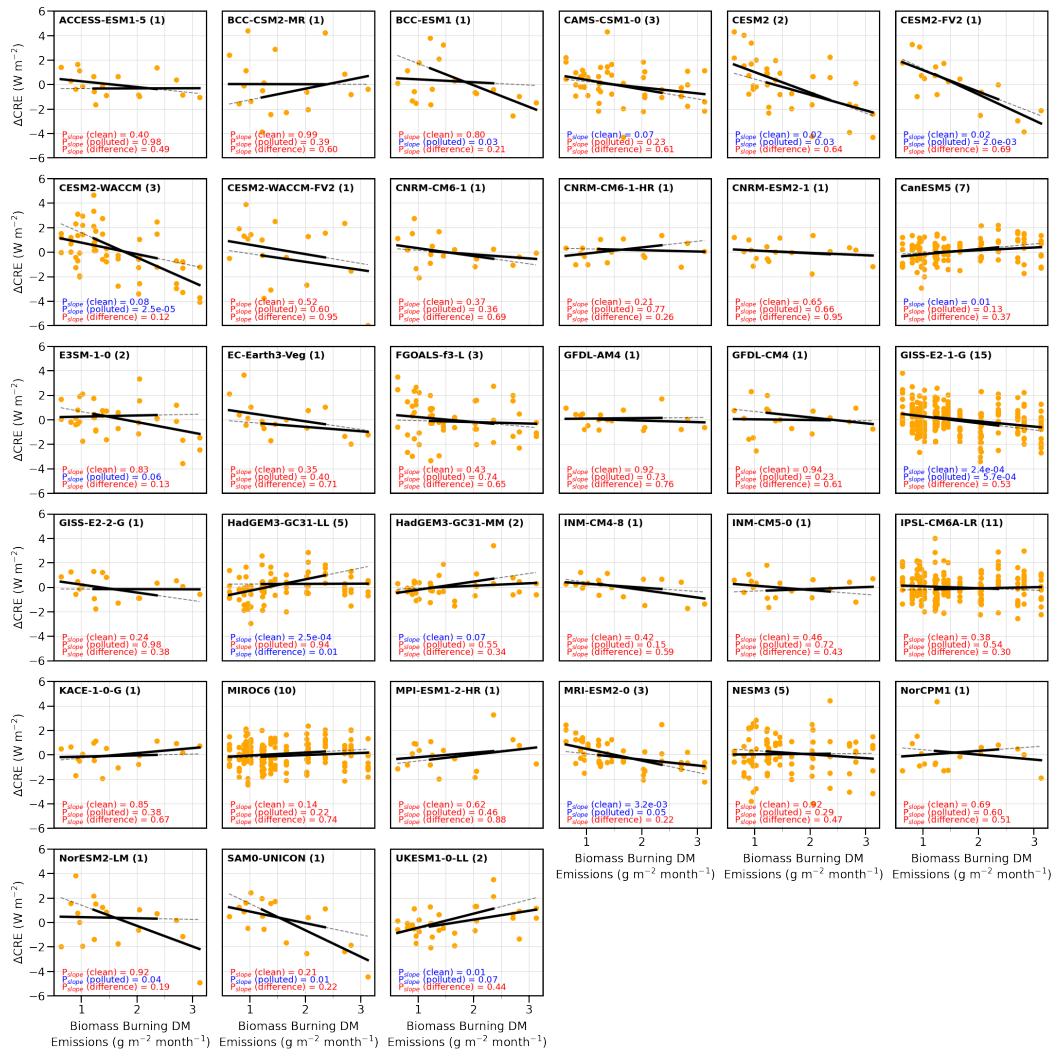
Figure S7. **Cloud radiative effect (CRE) response at varying biomass burning (BB) emissions averaged in CMIP6-AMIP models.** Shown is the CRE response to varying BB emissions (shown as dry matter (DM) emissions) averaged from 50–70°N from data submitted to the CMIP6-AMIP historical simulations from 1997–2014. The number of ensemble members used for each model are shown in parentheses. See Text S5 for further information on data sources. CRE anomalies are relative to the monthly mean values. Black lines show linear regressions of the 80% most clean and polluted aerosol concentrations. P_{slope} (clean and polluted) refer to to the P-value of whether the slope is significant from zero for the clean and polluted regressions, respectively. P_{slope} (difference) refers to the P-value of whether the clean and polluted slopes are significantly different from each other. P-values highlight in blue (red) are (are not) significant to 90% confidence.

January 5, 2023, 1:17am